1 **Warming impairs trophic transfer efficiency in a long-term field experiment**

2 Diego R Barneche[1,2,3], Chris J Hulatt[4,5], Matteo Dossena[4], Daniel Padfield[3], Guy Woodward[6],

3 Mark Trimmer[4,*], Gabriel Yvon-Durocher[3,*]

4 [1]Australian Institute of Marine Science, Indian Ocean Marine Research Centre, Crawley, WA 6009, Australia

5 [2]Oceans Institute, The University of Western Australia, Crawley, WA 6009, Australia

6 [3]Environment and Sustainability Institute, University of Exeter, Penryn, United Kingdom, TR10 9FE

7 [4]School of Biological and Chemical Sciences, Queen Mary University of London, London, United Kingdom

8 [5]Faculty of Biosciences and Aquaculture, Nord University, Bodø, Norway

9 [6]Department of Life Sciences, Imperial College London, Silwood Park, Buckhurst Road, Ascot, Berkshire, SL5
10 7PY, United Kingdom

11 [*]e-mail: `g.yvon-durocher@exeter.ac.uk` or `m.trimmer@qmul.ac.uk`.

12 **Running title:** Warming reduces trophic transfer efficiency

13 **Keywords:** nitrogen, carbon, stoichiometry, efficiency of energy transfer, phytoplankton, zoo-
14 plankton, stable isotopes, biomass

15 **Word count:** 2,030 (Text), 2,983 (Methods).

16 **Figures:** 3; **Text references:** 38; **Methods references:** 6.

17 **Extended Data Figures:** 9; **Extended Data Tables:** 1.

18 **Supplementary Figures:** 13; **Supplementary Tables:** 2.

In natural ecosystems, the efficiency of energy transfer from resources to consumers determines the biomass structure of food webs. As a general rule, about 10% of the energy produced in one trophic level makes it up to the next[1–3]. Recent theory suggests this energy transfer could be further constrained if rising temperatures increase metabolic growth costs[4], although experimental confirmation in whole ecosystems is lacking. We quantified nitrogen transfer efficiency (a proxy for overall energy transfer) in freshwater plankton in artificial ponds exposed to 7 years of experimental warming. We provide the first direct experimental evidence that, relative to ambient conditions, 4°C of warming can decrease trophic transfer efficiency by up to 56%. In addition, both phytoplankton and zooplankton biomass were lower in the warmed ponds, indicating major shifts in energy uptake, transformation and transfer[5,6]. These new findings reconcile observed warming-driven changes in individual-level growth costs and carbon-use efficiency across diverse taxa[4,7–10] with increases in the ratio of total respiration to gross primary production at the ecosystem level[11–13]. Our results imply that an increasing proportion of the carbon fixed by photosynthesis will be lost to the atmosphere as the planet warms, impairing energy flux through food chains, with negative implications for larger consumers and the functioning of entire ecosystems.

Energy transfer efficiency between trophic levels has been recognised as a key determinant of how biomass is distributed in ecosystems for more than a century[1–3,14–17]. More efficient energy transfer across short food chains can lead to higher standing biomass of upper trophic levels: for example, inverted biomass pyramids are often seen in aquatic food webs[18,19], where consumer stocks outweigh those of the smaller producers, with much higher biomass turnover rates than their animal consumers. At the other extreme, inefficient energy transfer via long food chains can explain the relatively low biomass of apex predators in other ecosystems[16,20,21]. Understanding how rising temperatures might alter the efficiency of energy transfer through food chains[22,23] is therefore critical for predicting how ecosystem structure and function will respond to global warming as well as for assessing impacts on commercially important apex predators, which are already under threat from a multitude of other stressors[24].

Multiple studies suggest that elevated temperatures decrease the carbon-use efficiency or increase growth costs for individuals[4,7–10] and recent theory demonstrates how higher growth

2

49 costs could reduce energy transfer efficiency through food chains[4]. Although a handful of stud-

50 ies have indirectly inferred that rising temperatures may be linked to declines in energy transfer

51 efficiency in different systems[22,23,25], direct experimental measurements have remained elusive.

52 We established an outdoor, still-water mesocosm experiment in 2005[17] to address this gap, us-

53 ing twenty 1 m^3 artificial ponds, half of which have been warmed by 4°C (e.g. in line with

54 IPCC Scenario A1B[26]) above ambient temperature since September 2006 (Extended Data Fig.

55 1). These ponds have been open to natural dispersal and colonisation from the regional species

56 pool for hundreds of generations and have well-established, diverse communities[27], allowing us

57 to explore how warming alters ecological and evolutionary dynamics in whole ecosystems. In

58 2013, after 7 years of warming, we carried out a ^{15}N isotope tracer experiment[28] to track how

59 long-term warming had altered the trophic transfer efficiency between phytoplankton and their

60 zooplankton consumers.

61 On the 16th July 2013, we added a trace amount (980 μmol) of K^{15}NO$_3$—hereafter the ^{15}N-

62 tracer—to sixteen ponds over the course of 24 hours (Extended Data Fig. 1). The experiment

63 was designed to trace the natural incorporation of nitrogen over time, but without perturbing the

64 system by inducing a phytoplankton bloom due to an artificial fertilisation effect. The addition

65 of the ^{15}N-tracer had no detectable influence on the concentration of total dissolved inorganic

66 nitrogen, nor did it affect the daytime CO_2 influx to the ponds through net primary production

67 (see Methods, Extended Data Figs. 2,3, Supplementary Table S1, Supplementary Figs. S1–4).

68 We quantified nitrogen transfer between phytoplankton and zooplankton as a proxy for overall

69 energy transfer based on our finding that the biomass C:N ratio of both plankton groups did not

70 vary systematically within each pond during the experiment (see Methods, Supplementary Fig.

71 S5). Because the C:N ratio within each pond remained constant while nitrogen was being assim-

72 ilated, we can conclude that carbon was assimilated proportionately, supporting the assumption

73 that the efficiency of carbon and energy transfer between trophic levels can be measured by

74 tracing nitrogen incorporation dynamics (see Methods). The ^{15}N-tracer was quantified in each

75 pond as ^{15}N$_{\%}$ (i.e. excess atom percent) relative to baseline throughout the experiment (54 days;

76 see Methods).

77 Using stable isotope tracers to understand material fluxes, and how they vary with environ-

78 mental gradients has a rich history in ecology[28–31]. We adapted a one-compartment, first-order

79 absorption model previously employed to model isotope incorporation in insects[29]. Here, the

80 dynamics of the tracer (i.e. incorporation up to the peak and decay after the peak) results from

81 the balance between an absorption, κ_a, and an elimination, κ_e, rate (d^{-1}). Specifically, the excess

82 ^{15}N$_‰$, χ, realised in the biomass pool at time t can be described as

$$\chi(t) = \frac{\phi\,\kappa_e\,\kappa_a\left(e^{-\kappa_e t} - e^{-\kappa_a t}\right)}{\kappa_a - \kappa_e}, \tag{1}$$

83 where ϕ (% d) is an empirical normalisation constant. We applied a Bayesian hierarchical ap-

84 proach to estimate ϕ, κ_a, and κ_e for each temperature treatment (ambient vs. warmed), while

85 accounting for pond-level variation (see Methods and Extended Data Fig. 4). The model cap-

86 tured the ^{15}N-tracer dynamics and revealed substantial differences between treatments for both

87 phytoplankton and zooplankton (Fig. 1, Extended Data Fig. 5, Supplementary Fig. S6). Phyto-

88 plankton rapidly incorporated the ^{15}N$_‰$ during the first few days of the experiment (Extended

89 Data Fig. 5), whereas its uptake by the zooplankton was slower and mirrored the tracer decay

90 in the phytoplankton, highlighting the close coupling of material transfer between these trophic

91 levels. Both response curves were asymmetric (Fig. 1), with a faster approach to the peak than

92 for the decay phase[29].

93 The absorption rate, κ_a, was unaffected by warming among the phytoplankton (ambient: median

94 = 0.61; 95% credible intervals (C.I.) = 0.35–0.89; warmed: median = 0.62; 95% C.I. = 0.33–

95 1.03), but was elevated among the zooplankton from the warmed ponds (median = 0.17; 95% C.I.

96 = 0.04–0.47) relative to ambient ponds (median = 0.08; 95% C.I. = 0.02–0.23; Fig. 2a, Extended

97 Data Table 1). The elimination rate, κ_e, however, was higher in the warmed ponds for both phy-

98 toplankton (ambient: median = 0.11; 95% C.I. = 0.05–0.22; warmed: median = 0.31; 95% C.I. =

99 0.13–0.55) and zooplankton (ambient: median = 0.09; 95% C.I. = 0.05–0.14; warmed: median

100 = 0.14; 95% C.I. = 0.06–0.26; Fig. 2b). These findings demonstrate that long-term warming

101 has fundamentally altered material flux dynamics in these plankton communities. The higher

102 rates of ^{15}N absorption and elimination in the zooplankton, as well as higher rates of elimina-

103 tion in the phytoplankton are consistent with faster metabolism at elevated temperatures[32,33].

104 Furthermore, the lack of a warming effect on the absorption rate, coupled with markedly faster

105 elimination in the phytoplankton, and the substantial effects of warming on the rates of both

106 processes in the zooplankton, is also consistent with the differential temperature sensitivities
107 of photosynthesis and respiration[5]. That is, nitrogen absorption in the phytoplankton is likely
108 linked to autotrophic metabolism and growth only, while nitrogen elimination in both the phy-
109 toplankton and zooplankton will also be influenced by rates of heterotrophic metabolism which
110 tend to have a higher temperature sensitivity[5,6,34,35].

111 Equation 1 shows that at time t, the ^{15}N-tracer present in the biomass pool will depend on the
112 balance between κ_a and κ_e: i.e., there are gains and losses throughout the curve. Thus, the
113 efficiency of nitrogen transfer, $\varepsilon(t)$, is calculable as the ratio between the tracer realised in the
114 biomass pool at time t relative to the entire tracer fraction that has been absorbed since day 0 up
115 to t

$$\varepsilon(t) = \frac{\chi(t)}{\phi \kappa_e \left(1 - e^{-\kappa_a t}\right)}. \tag{2}$$

116 We can then integrate equation 2 to quantify the mean efficiency of nitrogen transfer, $\bar{\varepsilon}$, over
117 the duration of the experiment, $\tau = 54$ days:

$$\bar{\varepsilon} = \frac{\int_{t=0}^{t=\tau} \varepsilon(t) dt}{\tau}. \tag{3}$$

118 For phytoplankton, $\bar{\varepsilon}$ reflects the efficiency of nitrogen uptake from the inorganic tracer pool
119 (including any recycled nitrogen through, e.g., zooplankton excretion), while for zooplankton
120 it quantifies nitrogen transfer efficiency from the phytoplankton. It is important to note that
121 equations 1–3 constitute a phenomenological characterisation of nitrogen incorporation dynam-
122 ics and transfer efficiency in that they make no attempt to mechanistically quantify the multi-
123 tude of physiological (e.g. nutrient uptake, respiration, excretion, photosynthesis), ecological
124 (e.g. predation, mortality, changes in biomass and species composition) and biogeochemical
125 (e.g. internal nutrient recycling) processes that ultimately influence the rates of nitrogen absorp-
126 tion, elimination and transfer efficiency within the phytoplankton and zooplankton. Rather, any
127 treatment effects that we observe in the model parameters κ_a and κ_e, and the efficiency $\bar{\varepsilon}$ re-
128 flect the emergent outcome of temperature-driven shifts in some or all of these physiological,
129 ecological and biogeochemical processes.

5

We obtained posterior distributions of treatment-specific mean efficiencies of nitrogen transfer, $\bar{\varepsilon}$, based on the treatment-specific Bayesian posterior distributions of κ_a, κ_e, and ϕ. $\bar{\varepsilon}$ ranged from 10–40% on average across treatments and groups (Fig. 2d), consistent with previous estimates from natural systems[2,3]. From the posterior draws of treatment-specific $\bar{\varepsilon}$, we also obtained a distribution of the percentage decline in $\bar{\varepsilon}$ between ambient and warmed ponds, which was substantially reduced in the warmed ponds for both the phytoplankton (median decline = 56.4%; upper 95% C.I. = 27.5–87.8%) and zooplankton (38.1%; upper 95% C.I. = 3.6–81.3%) communities (Fig. 2d; Extended Data Fig. 6). A Bayesian hierarchical model, which accounted for repeated measures throughout the experiment, revealed that biomass was lower in the warmed ponds (Fig. 3) for both phytoplankton (median decline = 58.4%; 95% C.I. = 22.9–84.0%) and zooplankton (65.6%; 95% C.I. = 12.8–93.2%), which is consistent with reduced energy transfer efficiency altering the biomass pyramid[17] (Extended Data Fig. 6, Supplementary Fig. S7).

Our findings show that the structure and functioning of the ecosystems that have emerged after 7 years of experimental warming are characterised by markedly lower trophic transfer efficiency compared with those that have assembled under ambient temperature regimes. A wide range of interrelated and non-mutually exclusive physiological, ecological and evolutionary mechanisms could provide causative explanations for these results, but such fine-grained processes cannot be disentangled in a field experiment with freely assembling ecosystems of the scale and complexity as presented in this study. Nevertheless, a number of lines of evidence provide important clues. For example, we have consistently observed that warming has shifted the phytoplankton communities towards larger species[17,27,36] (Supplementary Fig. S8) that are also potentially less palatable to zooplankton consumers. Such a shift in the edibility of the phytoplankton communities could at least partially explain the lower trophic transfer efficiency in the warmed ecosystems. In contrast, the metabolic balance quantifies the overall energy balance between photosynthesis (carbon fixation) and respiration (carbon remineralisation) at the ecosystem scale and throughout this long-term experiment we have observed that warming has increased the ratio of ecosystem respiration (ER) to gross primary production (GPP)[13,26] (see Supplementary Fig. S9). These results emphasise that despite shifts in taxonomic composition, the fundamental effect of warming in altering the carbon metabolism and energy balance of these

160 ecosystems has remained consistent. Thus, whilst the structural elements of the ecosystems may

161 have undergone reorganisation over time either via ecological change of the constituent taxa[17,27]

162 or via evolutionary adaptation[37], the thermodynamic impacts of warming on energy metabolism

163 seem to ultimately constrain the effects of rising temperatures on ecosystem functioning. The

164 findings in the present manuscript—that warming has decreased the efficiency of energy transfer

165 between trophic levels—appears to encapsulate yet another manifestation of the way in which

166 warming has radically altered the metabolism and energy flows in these ecosystems. Together

167 this body of evidence suggests that rising temperatures alter metabolism at the organism level

168 which, in turn, reduces the amount of energy that can be transferred from one trophic level to the

169 next. Ultimately this means that more of the carbon fixed by photosynthesis is respired and lost

170 to the atmosphere as heat and CO_2 with less being retained in the ecosystem. If these findings

171 are generally applicable—and there is good reason to believe they could be[22,23,25,38]—climate

172 warming could cause major changes to the flux of energy and declines in the biomass of top-

173 predators in the aquatic realm, which may impair the critical services that aquatic ecosystems

174 deliver to society, including the provision of food from commercial fisheries.

175 1. Semper, K. *Animal life as affected by the natural conditions of existence*. **30,** 488 (Appleton;

176 Co., 1881).

177 2. Lindeman, R. L. The trophic-dynamic aspect of ecology. *Ecology* **23,** 399–417 (1942).

178 3. Pauly, D. & Christensen, V. Primary production required to sustain global fisheries. *Nature*

179 **374,** 255–257 (1995).

180 4. Barneche, D. R. & Allen, A. P. The energetics of fish growth and how it constrains food-web

181 trophic structure. *Ecology Letters* **21,** 836–844 (2018).

182 5. Allen, A. P., Gillooly, J. F. & Brown, J. H. Linking the global carbon cycle to individual

183 metabolism. *Functional Ecology* **19,** 202–213 (2005).

184 6. Yvon-Durocher, G. *et al.* Reconciling the temperature dependence of respiration across

185 timescales and ecosystem types. *Nature* **487,** 472–476 (2012).

186 7. Schaum, C., Buckling, A., Smirnoff, N., Studholme, D. J. & Yvon-Durocher, G. Environmen-

187 tal fluctuations accelerate molecular evolution of thermal tolerance in a marine diatom. *Nature*

Communications **9,** 1719 (2018).

8. Manzoni, S., Taylor, P., Richter, A., Porporato, A. & Ågren, G. I. Environmental and stoichiometric controls on microbial carbon-use efficiency in soils. *New Phytologist* **196,** 79–91 (2012).

9. Bradford, M. A. & Crowther, T. W. Carbon use efficiency and storage in terrestrial ecosystems. *New Phytologist* **199,** 7–9 (2013).

10. Barneche, D. R., Jahn, M. & Seebacher, F. Warming increases the cost of growth in a model vertebrate. *Functional Ecology* **33,** 1256–1266 (2019).

11. Laws, E. A., Falkowski, P. G., Smith Jr., W. O., Ducklow, H. & McCarthy, J. J. Temperature effects on export production in the open ocean. *Global Biogeochemical Cycles* **14,** 1231–1246 (2000).

12. Davidson, E. A. & Janssens, I. A. Temperature sensitivity of soil carbon decomposition and feedbacks to climate change. *Nature* **440,** 165–173 (2006).

13. Yvon-Durocher, G., Hulatt, C. J., Woodward, G. & Trimmer, M. Long-term warming amplifies shifts in the carbon cycle of experimental ponds. *Nature Climate Change* **7,** 209–213 (2017).

14. Elton, C. S. *Animal ecology.* 260 (Macmillan Co., 1927).

15. Sheldon, R. W., Sutcliffe Jr., W. H. & Paranjape, M. A. Structure of pelagic food chain and relationship between plankton and fish production. *Journal of the Fisheries Research Board of Canada* **34,** 2344–2353 (1977).

16. Brown, J. H. & Gillooly, J. F. Ecological food webs: High-quality data facilitate theoretical unification. *Proceedings of the National Academy of Sciences* **100,** 1467–1468 (2003).

17. Yvon-Durocher, G., Montoya, J. M., Trimmer, M. & Woodward, G. Warming alters the size spectrum and shifts the distribution of biomass in freshwater ecosystems. *Global Change Biology* **17,** 1681–1694 (2011).

18. Gasol, J. M., del Giorgio, P. A. & Duarte, C. M. Biomass distribution in marine planktonic communities. *Limnology and Oceanography* **42,** 1353–1363 (1997).

215   19. Wang, H., Morrison, W., Singh, A. & Weiss, H. Modeling inverted biomass pyramids and
216   refuges in ecosystems. *Ecological Modelling* **220,** 1376–1382 (2009).

217   20. Hutchinson, G. E. Homage to Santa Rosalia or why are there so many kinds of animals?
218   *The American Naturalist* **93,** 145–159 (1959).

219   21. Post, W. M. & Pimm, S. L. Community assembly and food web stability. *Mathematical*
220   *Biosciences* **64,** 169–192 (1983).

221   22. Šolić, M. *et al.* Impact of the 3°C temperature rise on bacterial growth and carbon transfer
222   towards higher trophic levels: Empirical models for the Adriatic Sea. *Journal of Marine Systems*
223   **173,** 81–89 (2017).

224   23. Ullah, H., Nagelkerken, I., Goldenberg, S. U. & Fordham, D. A. Climate change could drive
225   marine food web collapse through altered trophic flows and cyanobacterial proliferation. *PLOS*
226   *Biology* **16,** 1–21 (2018).

227   24. Jackson, J. B. C. *et al.* Historical overfishing and the recent collapse of coastal ecosystems.
228   *Science* **293,** 629–637 (2001).

229   25. Stock, C. A. *et al.* Reconciling fisheries catch and ocean productivity. *Proceedings of the*
230   *National Academy of Sciences* **114,** E1441–E1449 (2017).

231   26. Yvon-Durocher, G., Jones, J. I., Woodward, G., Trimmer, M. & Montoya, J. M. Warming
232   alters the metabolic balance of ecosystems. *Philosophical Transactions of the Royal Society B:*
233   *Biological Sciences* **365,** 2117–2126 (2010).

234   27. Yvon-Durocher, G. *et al.* Five years of experimental warming increases the biodiversity and
235   productivity of phytoplankton. *PLOS Biology* **13,** 1–22 (2015).

236   28. Mulholland, P. J. *et al.* Food resources of stream macroinvertebrates determined by natural-
237   abundance stable C and N isotopes and a ^{15}N tracer addition. *Journal of the North American*
238   *Benthological Society* **19,** 145–157 (2000).

239   29. Crossley, Jr., D. A. & Reichle, D. E. Analysis of transient behavior of radioisotopes in insect
240   food chains. *BioScience* **19,** 341–343 (1969).

241   30. Mulholland, P. J. *et al.* Stream denitrification and total nitrate uptake rates measured using
242   a field ^{15}n tracer addition approach. *Limnology and Oceanography* **49,** 809–820 (2004).

243 31. López-Sepulcre, A. *et al.* A new method to reconstruct quantitative food webs and nutrient
244 flows from isotope tracer addition experiments. *The American Naturalist* **online early,** (2020).

245 32. Brown, J. H., Gillooly, J. F., Allen, A. P., Savage, V. M. & West, G. B. Toward a metabolic
246 theory of ecology. *Ecology* **85,** 1771–1789 (2004).

247 33. Gillooly, J. F., Brown, J. H., West, G. B., Savage, V. M. & Charnov, E. L. Effects of size
248 and temperature on metabolic rate. *Science* **293,** 2248–2251 (2001).

249 34. Gillooly, J. F. *et al.* The metabolic basis of whole-organism RNA and phosphorus content.
250 *Proceedings of the National Academy of Sciences* **102,** 11923–11927 (2005).

251 35. Allen, A. P. & Gillooly, J. F. Towards an integration of ecological stoichiometry and the
252 metabolic theory of ecology to better understand nutrient cycling. *Ecology Letters* **12,** 369–384
253 (2009).

254 36. Padfield, D., Buckling, A., Warfield, R., Lowe, C. & Yvon-Durocher, G. Linking phyto-
255 plankton community metabolism to the individual size distribution. *Ecology Letters* **21,** 1152–
256 1161 (2018).

257 37. Schaum, C. *et al.* Adaptation of phytoplankton to a decade of experimental warming linked
258 to increased photosynthesis. *Nature Ecology & Evolution* **1,** 0094 (2017).

259 38. Rosenberg, A. A. *et al. Developing new approaches to global stock status assessment and
260 fishery production potential of the seas*. **1086,** 175 (FAO, 2014).

Figure legends

Fig. 1 | Temporal dynamics of the ^{15}N-tracer, χ (excess ^{15}N$_\%$), during the experiment. a, mean predicted curves for phytoplankton and **b,** zooplankton. Solid lines represent mean treatment-specific (ambient, blue vs. warmed, red) predicted curves which were obtained by fitting equation 1 to the data via a non-linear hierarchical model using a Bayesian model (see Methods). See Extended Data Fig. 5 and Supplementary Fig. S6 for pond-level mean model fits to the data and posterior predictive checks. Shaded polygons represent Bayesian 95% credible intervals which were calculated from 20,000 posterior draws. Silhouettes: ©Diego Barneche.

Fig. 2 | Impacts of long-term warming on the parameters that determine ^{15}N-tracer dynamics (equation 1), and the mean efficiency of nitrogen transfer (equation 3). a, absorption rate, κ_a, **b,** elimination rate, κ_e, **c,** empirical constant, ϕ, and **d,** mean efficiency of nitrogen transfer, $\bar{\varepsilon}$. Treatment-level (ambient, blue vs. warmed, red) parameter estimates (**a**–**c**) were obtained by fitting equation 1 to the data via a non-linear hierarchical Bayesian model (see Methods). Efficiency (**d**) was calculated over $\tau = 54$ days (duration of the experiment) based on equations 2 and 3, using the treatment-level parameter estimates. Density polygons represent Bayesian 99% credible intervals (C.I.) which were calculated from 20,000 posterior draws. Left panels: phytoplankton; right panel: zooplankton. Silhouettes: ©Diego Barneche.

Fig. 3 | Impacts of long-term warming on plankton community biomass. Mean biomass estimates were calculated from ambient (blue) and warmed (red) ponds ($n = 8$ per treatment). y-axis is log-scaled. Points represent mean carbon biomass for each pond calculated over the entire duration of the ^{15}N-tracer experiment (see Methods). Boxplots depict the median (mean line), as well as the first and third quartiles (lower and upper hinges). Error whiskers represent up to 1.5 times the the inter-quartile range (i.e. distance between the first and third quartiles) beyond the hinges. Shapes represent phytoplankton (top, circles) and zooplankton (squares, bottom). Silhouettes: ©Diego Barneche.

Methods

Experimental set up

Mesocosm pond facility. The facility was established in 2005 and consists of 20 artificial ponds of about $1m^3$ volume, 50 cm depth, sited in southern England (Freshwater Biological Association River Laboratory, East Stoke, 2°10'W, 50°13'N), designed to be broadly representative of mid-latitude shallow standing waters[17]. Warming of 4–5°C above ambient began in half of the ponds in September 2006 by maintaining a constant differential between thermocouples in a pair of warmed and ambient ponds (Extended Data Fig. 1). The choice of 4°C for the warmed treatment was based on the IPCC Scenario A1B for temperate regions of the Northern hemisphere[26,39].

The warming treatment has been continuously maintained until the present (May 2020). We categorise the duration of the experiment as "long-term" because it encompasses enough time for ecological, evolutionary and ecosystem successional dynamics to play out. Seven years (the duration of the experiment at the time of the tracer additions) encompasses many hundreds to thousands of generations for the planktonic organisms studied here. This means that the emergent outcomes we are measuring in these systems encompass both the immediate physiological impacts of warming, as well as the changes due to local extinctions and colonisation dynamics (ecological turnover) and genetic changes in the constituent taxa as they adapt (evolutionary dynamics) to the new environmental conditions imposed by the experimental treatments[17,27,36,37].

Taxonomic composition. The pool of species available for initial colonisation was standardised at the outset by seeding all of the ponds in December 2005 with a "common garden" inoculum of organisms from surrounding freshwater habitats. The ponds were then left open to natural colonisation and dispersal and now contain diverse multi-trophic communities that include macrophytes, macroinvertebrates[40], microbes, phytoplankton and zooplankton[17,27]. The composition and biomass structure of these communities in the warmed and ambient treatments have diverged substantially over the course of the experiment[17,27,36] (see Supplementary Fig. S8).

¹⁵N-tracer Experiment. The tracer experiment ran from the 10th of July 2013 to 8th of September 2013. Before the ¹⁵N-tracer experiment started a representative sample of the entire community was collected from each of the 20 ponds. Over the course of 24 hours, starting on the 16th of

315 July 2013, 16 of the 1000 L ponds (8 warmed and 8 ambient) each received a total of 980 μmol

316 of K^{15}NO$_3$ (98 Atom%, Sigma-Aldrich) from a 20 mmol L^{-1} stock solution. The ^{15}N-tracer was

317 added in 10 aliquots of 5 mL stock solution diluted in approximately 10 L of pond water trickled

318 over the surface of the same pond using a watering can. Each aliquot of ^{15}N-tracer was equiva-

319 lent to ~ 0.1 μmol ^{15}NO$_3^-$ L^{-1} in each pond to a total of ~ 1 μmol ^{15}NO$_3^-$ L^{-1} over 24 hours.

320 The across-time and across-pond means of dissolved inorganic nitrogen (DIN = NO$_2^-$ + NO$_3^-$

321 + NH$_4^+$) was 2.87 μmol L^{-1} $\pm$ 0.5 (S.E.). Addition of the ^{15}N-tracer had no discernible effect on

322 the concentration of dissolved inorganic nitrogen and the daytime CO$_2$ influx (Extended Data

323 Figs. 2,3). A further 3 of the remaining ponds were not treated, but were used as controls for

324 ^{15}N addition (Extended Data Fig. 7).

325 The water column of the ponds was sampled using a 4 L plastic tube open at both ends, the

326 tube was gently sunk through the water column until it reached the bottom and then closed on

327 both ends. Duplicate samples were taken from each pond so that both open water and areas

328 with macrophytes were sampled; these were then mixed and immediately taken to the on-site

329 laboratory.

330 In the laboratory, samples were sieved through a 50 μm nylon mesh to isolate zooplankton. The

331 < 50 μm fraction was filtered through a pre-ashed Whatman GF/F filter (0.7 μm nominal pore

332 size) in duplicate to isolate the phytoplankton fraction (verified by microscopy); the contents

333 of each fraction was gently rinsed with clean particulate-free water to remove any excess of

334 ^{15}N-tracer enriched water. The GF/F and a 30 mL sub-sample of water filtered at 0.7 μm were

335 immediately frozen at -20˚C for inorganic nutrient analysis (see below), whilst the >50 μm

336 fraction was re-suspended in clean water and the zooplankton kept alive at room temperature to

337 allow gut evacuation and sedimentation of the debris. After a few hours, the zooplankton were

338 separated from water and debris and then frozen at -20˚C.

339 Samples were collected with a decreasing frequency so that 4 sets of 16 samples of each fraction

340 were taken over the first 48 hours, starting from the addition of the first ^{15}N-tracer aliquot; then

341 one set per day was taken for the following three days; one set per week for the following month;

342 and a final set taken a month after the last sample.

343 Following the experiment, samples were analysed using a Sercon Integra 2 Isotope Ratio

344 Mass Spectrometer (IRMS). Samples of the zooplankton fraction were quickly defrosted

345 by re-suspension in ultra-pure water and all individuals were collected under a dissection

346 microscope using forceps, placed directly in pre-weighted ultraclean tin caps (6 mm × 4 mm,

347 Elemental Microanalysis, UK), dried (48 hours, 60˚C) and weighed on a Mettler Toledo MX5

348 precision balance. Phytoplankton samples were dried to a constant weight (48 hours, 60˚C),

349 and the dry weight of particulate matter on the filter used to calculate and standardise the

350 sample mass for IRMS. Phytoplankton sub-samples were prepared by coring the GF/F filters

351 and samples contained 14.9 μg N on average.

352 Samples were assembled in batches of 60 to 100 similar sample weight and each of these batches

353 were analysed by IRMS. Two types of certified reference materials were used for this analysis:

354 Casein (δ^{15}N +5.94‰, 13.32% Nitrogen, 46.5% Carbon) and EMA (δ^{15}N -1.57‰, 7.46% Ni-

355 trogen, 68.35% Carbon) (Elemental Microanalysis, UK). Casein was used for calibration of all

356 samples. EMA was used to confirm calibration performance. Each batch of samples analysed by

357 IRMS contained a range of urea standards covering the range of sample weights in each batch:

358 first, 4 samples of the same reference material, then 4 samples of non-enriched urea δ^{15}N $\approx$

359 0.0‰ and finally 4 samples of enriched urea δ^{15}N = 1000‰.

360 **Data processing.** For each sample, we converted the abundance of heavy nitrogen, δ^{15}N (‰)[28],

361 into atom percent, ^{15}N$_\%$, as

$$\delta^{15}\text{N} = \left[\frac{R_s}{R_a} - 1\right] 1000$$

(4)

$$^{15}\text{N}_\% = 100 \frac{\delta^{15}\text{N} + 1000}{\delta^{15}\text{N} + 1000 + \left(\frac{1000}{R_a}\right)},$$

362 where R_s and R_a = 0.00367647 are respectively the ^{15}N:^{14}N ratios of the sample and the atmo-

363 sphere. For each sample, we calculated excess ^{15}N$_\%$ over baseline abundance (i.e. χ in equation

364 1) by subtracting the natural abundance values for each taxon, in each pond, measured 7 days

365 before the addition of the K^{15}NO$_3$ tracer.

366 **CO$_2$ and dissolved inorganic nitrogen.** Daytime CO$_2$ influx (μmol m^{-2} d^{-1}) was measured

367 daily in each pond using multiplexed automatic gas flux chambers (LI8100 & LI8150, Li-Cor)

368 with an infra-red gas analyser as described in ref.[13]. We used fluxes integrated across the day-

369 light absorption phase (i.e. influx) because those encompass the period within which phyto-

370 plankton are actively photosynthesising[13]. Dissolved inorganic nitrogen species (NO_2^-, NO_3^-,

371 NH_4^+) were measured with a Skalar San^{++} continuous flow auto-analyser and standard colori-

372 metric methods as described in ref.[41].

Model framework

374 **Model development.** We adapted equation 1 in the main text from a one-compartment first-

375 order absorption model which has been previously used to trace stable isotope incorporation in

376 animal models[29]. This model can be employed to characterise either the mass, m, or concentra-

377 tion, c (mass / volume), of a stable isotope in a particular compartment (e.g. phytoplankton or

378 zooplankton) of interest at time t. The model is generally formulated as

$$m(t) = \frac{m_0 \kappa_a \left(e^{-\kappa_e t} - e^{-\kappa_a t}\right)}{\kappa_a - \kappa_e}$$

(5)

$$c(t) = \frac{m_0 \kappa_e \kappa_a \left(e^{-\kappa_e t} - e^{-\kappa_a t}\right)}{\theta \left(\kappa_a - \kappa_e\right)},$$

379 where m_0 is the mass of tracer added to the ponds on time $t = 0$, and $\theta = v\kappa_e$ is the clearance

380 rate (volume / time), with v representing the compartment biovolume. It follows from this type

381 of model that the mass of the ^{15}N-tracer, m_0, will be absorbed at an exponential rate; thus, we

382 can calculate the mass of the ^{15}N-tracer that was absorbed into the compartment since time 0

383 as $m_a(t) = m_0(1 - e^{-\kappa_a t})$, such that $m_a(t) \equiv m_0$ when t is large—this assumes that m_0 is 100%

384 absorbable.

385 It is important to emphasise that equation 1 is a *phenomenological* adaptation of equation 5,

386 tailored to describe the dynamics of excess ^{15}N$_\%$, χ, observed in our experiment. As noted in

387 the main text, parameters κ_a and κ_e emerge from multiple potential physiological and ecological

388 processes that cannot be disentangled with this type of experiment. Moreover, a clearance rate

389 is impractical to determine because v represents the (unknown) biovolume of phytoplankton and

390 zooplankton. Therefore, in equation 1, we collapsed the ratio m_0/θ into the empirical constant,

391 ϕ, noting that its units (% d) are different because $\chi(t)$ in equation 1 is expressed as an excess

392 atom percent rather than concentration or mass as in equation 5 above. It also follows that the

393 product $\phi\kappa_e$ is analogous to the ratio m_0/v. We empirically demonstrate in the online Supple-

394 mentary information how we can quantify the efficiency of ^{15}N transfer at time t (i.e. equation

395 2) using three equivalent expressions.

396 **Model fitting.** We adopted a hierarchical model based on equation 1, which was implemented

397 in a Bayesian framework using the R package *rstan*[42] version 2.21.3 to determine posterior dis-

398 tributions and associated 95% credible intervals (C.I.) for the fitted parameters (Extended Data

399 Fig. 4). We fitted two models, one for each group (i.e. phyoplankton and zooplankton). Pa-

400 rameters κ_a, κ_e and ϕ were sampled from m treatment-level distributions (warmed vs. ambient),

401 and additional uncertainty within each of these distributions was estimated at the pond level, j

402 $= \{1–8\}$, within each treatment (i.e. 8 ponds per treatment; see Extended Data Fig. 4). A series

403 of transformations were adopted to improve convergence and run speed; (1) κ_a was estimated

404 on the natural log scale, such that pond-level $\kappa_{a[m,j]} = \exp(\overline{\ln\kappa_{a[m]}} + \ln\Delta\kappa_{a[m,j]})$; (2) to ensure

405 the constraint $\kappa_e < 1$, κ_e was estimated using a logit transformation, κ'_e, such that pond-level

406 $\kappa_{e[m,j]} = 1/(1 + \exp(-(\overline{\kappa'_{e[m]}} + \Delta\kappa'_{e[m,j]})))$; (3) convergence was achieved by enforcing the con-

407 straint $\phi < 1 / \kappa_e$ (i.e. assuming $\theta \ll v$ and $\kappa_e < 1$ in equation 5), hence ϕ was estimated using

408 a logit transformation, ϕ'; (4) for phytoplankton, ϕ was calculated from ϕ' and transformed to

409 the natural log scale, such that pond-level $\phi_{[m,j]} = \exp(\overline{\ln\phi_{[m]}} + \Delta\ln\phi_{[m,j]})$; (5) for zooplankton,

410 pond-level $\phi_{[m,j]} = (1/\kappa_{e[m,j]})/(1 + \exp(-(\overline{\phi'_{[m]}} + \Delta\phi'_{[m,j]})))$.

411 We used treatment and group-agnostic, weakly informative priors (Extended Data Fig. 4; Sup-

412 plementary Fig. S10) for all parameters. For the treatment-level means $\overline{\ln\kappa_{am}}$, $\overline{\kappa'_{em}}$ and $\overline{\phi'_m}$,

413 we used $\mathcal{N}(0,1)$. Pond-level hierarchical deviations from treatment-level means ($\ln\Delta\kappa_{a[m,j]}$,

414 $\Delta\kappa'_{e[m,j]}$, $\Delta\ln\phi_{[m,j]}$, $\Delta\phi'_{[m,j]}$) were assumed to be normally distributed with means of 0, thus the

415 treatment-level means ($\overline{\ln\kappa}$, $\overline{\kappa'_e}$, $\overline{\ln\phi}$, $\overline{\phi'}$) are among-pond means: $\ln\Delta\kappa_{a[m,j]} \sim \mathcal{N}(0,\sigma_{\ln\Delta\kappa_a})$,

416 $\Delta\kappa'_{e[m,j]} \sim \mathcal{N}(0,\sigma_{\Delta\kappa'_e})$, $\Delta\ln\phi_{[m,j]} \sim \mathcal{N}(0,\sigma_{\Delta\ln\phi})$, $\Delta\phi'_{[m,j]} \sim \mathcal{N}(0,\sigma_{\Delta\phi'})$. For the hyper priors

417 $\sigma_{\ln\Delta\kappa_a}$, $\sigma_{\Delta\kappa'_e}$, $\sigma_{\Delta\ln\phi}$ and $\sigma_{\Delta\phi'}$, we used $\Gamma(2,0.1)$.

418 The posterior distributions of model parameters (Extended Data Table 1) were estimated using

419 Markov chain Monte Carlo (MCMC) methods by constructing four chains of 30,000 steps each,

16

420 with each starting at a distinct point drawn at random from the prior distributions. Most of these

421 iterations (25,000) were used as a warm-up, so a total of 20,000 steps were retained to estimate

422 posterior distributions (i.e. $4 \times (30{,}000 - 25{,}000) = 20{,}000$). All four independent chains reached

423 convergence, i.e. the Gelman-Rubin statistic[43], $\widehat{R}$, was 1.

Linking nitrogen to carbon and energy transfer efficiency

425 We used a ^{15}N-tracer to quantify material transfer between trophic levels in the plankton food

426 web, assuming that our measurements of the efficiency of nitrogen transfer also reflect carbon

427 and energy transfer between trophic levels. To verify this assumption, we first tested whether

428 there were any within-pond temporal changes in C:N ratio in the ambient and warmed ponds by

429 fitting a Bayesian hierarchical linear model to each group (phytoplankton and zooplankton). If

430 over the duration of the 54 day experiment, which encompassed several turnovers in the short-

431 lived phyto- and zooplankton communities, the C:N ratio remained constant while nitrogen was

432 being assimilated, then we can conclude that carbon was being assimilated proportionately. We

433 included a fixed-effect interaction between time (continuous: day) and treatment (categorical:

434 ambient vs. warmed), and a pond-level random effect to account for repeated measures through-

435 out the experiment. C:N ratios were calculated based on moles of carbon and nitrogen in each

436 sample on each day. A time slope, β_t, that is indistinguishable from 0 would be considered

437 as evidence of no change in C:N ratio over the ^{15}N-tracer experiment, and our results support

438 this assumption: C:N ratio did not change over time for both phytoplankton (β_t for ambient

439 treatment: -0.02; Bayesian 95% C.I. = -0.08–0.03; β_t for warmed treatment: -0.03; 95% C.I.

440 = -0.08–0.03) or zooplankton (β_t for ambient treatment: -0.01; 95% C.I. = -0.04–0.02; β_t for

441 warmed treatment: 0.02; 95% C.I. = -0.01–0.04). These results reflect the fact that carbon

442 biomass differences between treatments (Fig. 3) mirror those of nitrogen biomass (Extended

443 Data Fig. 8). Pond-level C:N ratio means are shown in Extended Data Fig. 9. Together, these

444 lines of evidence support our key assumption that the assimilation and trophic transfer of nitro-

445 gen can be used as a direct proxy for the assimilation and transfer of carbon and energy.

446 We then tested whether there was a decline in plankton carbon biomass between ambient and

447 warmed treatments (Fig. 3 in the main text) that would be consistent with a decline in the effi-

448 ciency of energy transfer, by fitting a Bayesian hierarchical linear model to the biomass estimates

449 for each group. We included treatment (ambient vs. warmed) as a fixed effect, and pond as a

450 random effect to account for repeated measures throughout the experiment. Biomass data were

451 normalised by applying a natural-logarithm transformation. One of the samples presented an un-

452 usually high carbon biomass of phytoplankton (10-fold higher than the mean; Fig. 3) and was

453 therefore removed from the analysis. We used the posterior distribution of estimated parameters,

454 β_w (mean carbon biomass from warmed treatments) and β_a (mean carbon biomass from ambi-

455 ent treatments), to calculate a posterior distribution of between-treatment percentage decline for

456 both groups: $(1 - (\beta_w / \beta_a)) \times 100$. These distributions were overlaid on the percentage-decline

457 posterior distributions obtained for the efficiency of nitrogen transfer described in the main text.

458 For phytoplankton, the posterior distribution of carbon biomass % decline is virtually identical

459 to that of the percentage-decline in the efficiency of nitrogen transfer. For zooplankton, there

460 were subtle differences in means although the distributions overlapped over most of the range

461 (Extended Data Fig. 6). These data provide clear evidence of a decline in plankton biomass

462 between ambient and warmed treatments that is consistent with an impaired energy transfer

463 efficiency.

464 Models were fitted using the R package *brms*[44] version 2.14.4. Priors were uninformative (*brms*

465 default), and fitting specifications (number of chains, warm-up period) and convergence crite-

466 rion are the same as described above for equation 1.

467 **Before-after analyses**

468 We ran multiple before-after analyses to test whether the addition of the tracer had a discernible

469 effect on the dynamics of nitrogen incorporation in the plankton, and whether that exhibited

470 any interactions with the temperature treatment. Multiple dissolved inorganic nitrogen species

471 (NO_2^-, NO_3^-, NH_4^+; Extended Data Fig. 2) as well as daytime CO_2 influx (Extended Data

472 Fig. 3) were used as response variables, each in a separate model. For dissolved inorganic nitro-

473 gen species, measurements were compared between treatments and time periods (10th–15th July

474 2013 = "before"; 17th July–06th August = "after") which were designated relative to the addition

475 of the ^{15}N-tracer on the 16th of July 2013. For daytime CO_2 influx, measurements were taken

476 throughout the week "before" (9th–15th), and "after" (17th–23th) the addition of the ^{15}N-tracer.

477 We fitted the before-after model as an interaction between period (before, after) and treatment

478 (warm, ambient) using a Bayesian hierarchical approach, with pond added as an intercept-level

479 random effect. The before-after model was fitted using the R package *brms*[44] version 2.14.4.

480 Priors were uninformative (*brms* default), and fitting specifications (number of chains, warm-

481 up period) and convergence criterion are the same as described above for equation 1. The test

482 revealed no discernible interaction between treatment and period for any of the dissolved inor-

483 ganic nitrogen species nor daytime CO_2 influx (Extended Data Figs. 2,3; Supplementary Table

484 S1).

Main model residual analysis

486 We tested whether other physico-chemical properties besides temperature could be affecting the

487 variability in the tracer incorporation dynamics. To do so, we first calculated the mean posterior

488 observation-level residuals from our main model for each taxonomic group (i.e. phytoplankton

489 and zooplankton; Fig. 1; Extended Data Fig. 5; Extended Data Table 1). Then, for each group

490 separately, we employed a Bayesian hierarchical model to investigate the relationship between

491 the residuals from the original model and the dissolved inorganic nitrogen species (DIN = NO_2^-,

492 NO_3^-, NH_4^+) in the ponds. The model accounted for the repeated measurements at the pond

493 level as hierarchical effects both on the intercept and slopes of DIN species. The model was

494 fitted using the R package *brms*[44] version 2.14.4. Priors were uninformative (*brms* default),

495 and fitting specifications (number of chains, warm-up period) and convergence criterion are the

496 same as described above for equation 1. Results indicate that the DIN species could not explain

497 any systematic variation in our main model residuals (Supplementary Table S2; Supplementary

498 Figs. S11–13). That is, the main statistical analysis in our manuscript identifies a strong, main

499 effect of temperature that is not improved by adding the effect of inorganic nutrients.

Data and Code Availability

501 All data and R code (data manipulation, analyses, figures and tables) can be downloaded from

502 a GitHub repository (`https://github.com/dbarneche/nature20200508666`). When using

503 the data or code from this project, please cite it as "Barneche DR, Hulatt CJ, Dossena M, Pad-

504 field D, Woodward G, Trimmer M, Yvon-Durocher G (2021) dbarneche/nature20200508666:

505 Accepted version of paper data and code of manuscript: Warming impairs trophic transfer effi-

506 ciency in a long-term field experiment (Nature). Zenodo. doi: 10.5281/zenodo.4468371"

507 39. IPCC. in *Contribution of Working Group I to the fourth assessment report of the Intergov-*
508 *ernmental Panel on Climate Change* (eds. Parry, M. L., Canziani, O. F., Palutikof, J. P., van
509 der Linden, P. J. & E, H. C.) 7–22 (Cambridge University Press, 2007).

510 40. Dossena, M. *et al.* Warming alters community size structure and ecosystem functioning.
511 *Proceedings of the Royal Society B: Biological Sciences* **279,** 3011–3019 (2012).

512 41. Lansdown, K. *et al.* Importance and controls of anaerobic ammonium oxidation influenced
513 by riverbed geology. *Nature Geoscience* **9,** 357–360 (2016).

514 42. Stan Development Team. RStan: The R interface to Stan. (2020).

515 43. Gelman, A. & Rubin, D. B. Inference from iterative simulation using multiple sequences.
516 *Statistical Science* **7,** 457–472 (1992).

517 44. Bürkner, P. Advanced Bayesian multilevel modeling with the R package brms. *The R Jour-*
518 *nal* **10,** 395–411 (2018).

525 **Author contributions** G.Y.D. and M.T. conceived the study; C.J.H. and M.D. collected the data
526 and did the stable isotope analysis; D.P. collected the phytoplankton community data from 2016;
527 D.R.B., G.Y.D., and M.T. conducted the statistical analyses; D.R.B. and G.Y.D. wrote the first
528 version of the manuscript and all authors contributed substantially to revisions.

529 **Competing interests** The authors declare no competing interests.

530 **Additional information**

531 **Supplementary information** is available for this paper.

532 **Correspondence and requests for materials** should be addressed to G.Y.D. and M.T.

Extended Data

Extended Data Table 1 | Parameter estimates from equation 1, which characterises the temporal dynamics of the ^{15}N-tracer. Mean parameter estimates, 95% credible intervals (lower and upper bound), effective sample size, and Gelman-Rubin statistic[43], $\widehat{R}$, were obtained using a Bayesian hierarchical model. Parameter notation and model fitting approach are described in subsection *Model framework* of Methods. "amb" = ambient temperature; "war" = warmed (+4˚C) relative to ambient temperature. Overall treatment- and group-level model fits are visually depicted in Fig. 1; pond-level model fits are depicted in Extended Data Fig. 5.

Extended Data Figure 1 | Schematic of experimental pond set-up and ^{15}N-tracer measure-ments. a, Twenty artificial ponds, with 10 warmed (red) by 4˚C above (since September 2006) 10 ambient (blue) ponds, were paired in a randomized block design. **b,** Ponds were controlled via two temperature sensors, a heating element (HE) a thermostat (T-stat) and a solid-state relay (SSR). **c,** Timeline of experimental measurements, including quantification of baseline ^{15}N$_{\%}$ of phytoplankton and zooplankton before the addition of the K^{15}NO$_3$ tracer, followed by continu-ous sampling of excess ^{15}N$_{\%}$ relative to baseline on each pond. **d,** Dissolved oxygen saturation and pH did not change before and after the addition of the tracer (see ref.[13] for measurement details). Symbols represent treatments: ambient (blue triangles) and warmed (red inverted tri-angles). Silhouettes: ©Diego Barneche.

Extended Data Figure 2 | Concentration of dissolved inorganic nitrogen species in the ponds before and after the addition of the ^{15}N-tracer on the 16th July 2013. Addition of the ^{15}N-tracer had no discernible effect on the natural concentration of dissolved inorganic ni-trogen in the ponds (Supplementary Table S1). Points are treatment-level means, error bars are 95% confidence intervals. Dashed line marks 16th July.

Extended Data Figure 3 | Daytime CO$_2$ influx before and after the addition of the ^{15}N-tracer on the 16th July 2013. Each point represents an individual measurement within a pond ($n = 56$ measurements per treatment per period; as described in detail in ref.[13]). Colours refer to ambient (blue triangles) and warmed (red inverted triangles) ponds. "Before" measurements were taken daily throughout the week leading to the addition of the ^{15}N-tracer on the 16th of July 2013 (9th–15th), whereas "After" measurements were taken daily throughout the week following the addition of the tracer (17th–23th). Boxplots depict the median (mean line), as well as the first and third quartiles (lower and upper hinges). Error whiskers represent up to 1.5 times the the inter-quartile range (i.e. distance between the first and third quartiles) beyond the hinges. Outliers were removed from the plot for visualisation purposes only. A before-after analysis (see Supplementary Table S1) revealed no substantial changes in daytime CO$_2$ influx and net primary production due to the addition of the ^{15}N-tracer.

Extended Data Figure 4 | Hierarchical model structure for the fitting of equation 1. Data, processes and parameters are explicitly identified, with equation 1 parameters ϕ, κ_a and κ_e being fitted at the treatment level with pond-level deviations. Phytoplankton and zooplankton

silhouettes depict whether a certain transformation or prior was used for either group or both (see Methods). Silhouettes: ©Diego Barneche.

Extended Data Figure 5 | Temporal dynamics of the ^{15}N-tracer, χ (excess ^{15}N$_‰$), in phyto-plankton and zooplankton during the experiment. Dashed lines represent mean pond-level predictions which were obtained by fitting the data to equation 1 via a non-linear hierarchical Bayesian model (see Methods). Shaded polygons represent Bayesian 95% credible intervals which were calculated from 20,000 posterior draws. Note the sharp increase in the $\chi(t)$ in the first few days of the experiment, particularly when compared to baseline ^{15}N$_‰$ in the control ponds (Extended Data Fig. 7).
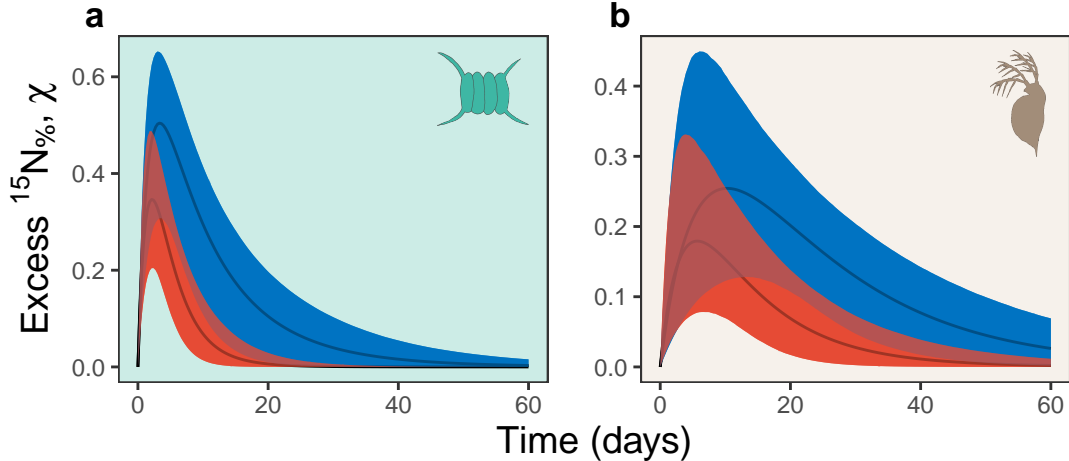
Extended Data Figure 6 | Posterior distributions of percentage decline in carbon biomass (μg C L^{-1}) and efficiency of nitrogen transfer due to long-term warming. Distributions were calculated using 20,000 posterior draws which were estimated via Bayesian hierarchical linear models (see Methods). Positive and negative values represent percentage decline and increase respectively. The strong overlap between distributions corroborates the assumption that mean nitrogen transfer efficiency, $\bar{\varepsilon}$, as calculated from the ^{15}N-tracer dynamics (equation 3), reflects the efficiency of carbon and hence energy transfer. Silhouettes: ©Diego Barneche.
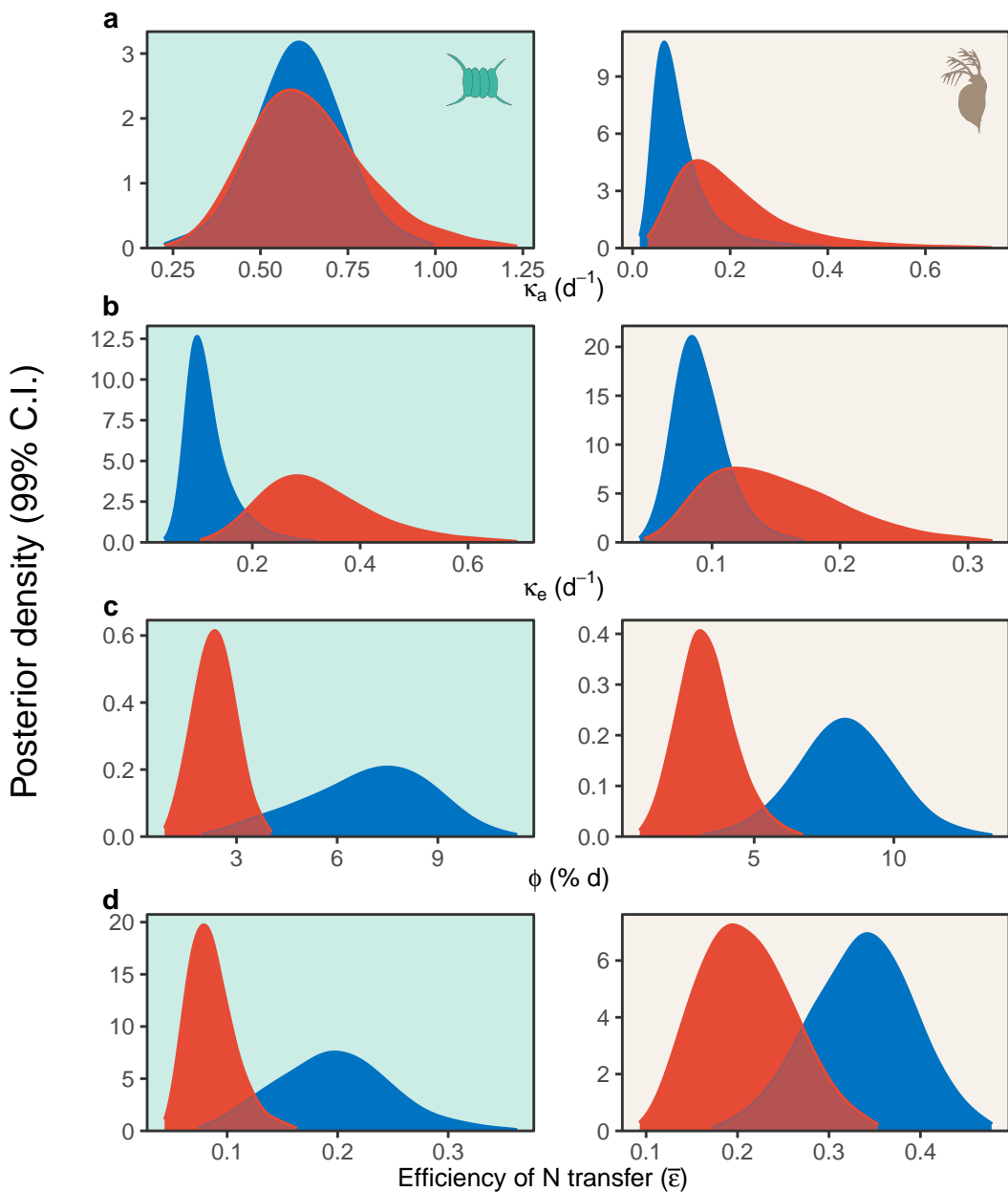
Extended Data Figure 7 | Measurements of ^{15}N$_‰$ (atom percent) in three untreated control ponds. Green circles represent phytoplankton ($n = 5$ per pond), whereas brown squares represent zooplankton ($n = 3$–5 per pond). These results are expected given that no tracer was added. The y-axis was kept fixed in order to compare the magnitude of change between treatments (see Extended Data Fig. 5) and controls. Refer to the Methods section for further explanations about how the data were collected.

Extended Data Figure 8 | Impacts of long-term warming on mean nitrogen biomass. Mean biomass nitrogen estimates were calculated from ambient and warmed ponds. Points represent means calculated for the entire duration of the ^{15}N-tracer experiment ($n = 8$ per treatment). Boxplots depict the median (mean line), as well as the first and third quartiles (lower and upper hinges). Error whiskers represent up to 1.5 times the the inter-quartile range (i.e. distance between the first and third quartiles) beyond the hinges. Shapes represent phytoplankton (top, circles) and zooplankton (squares, bottom). Silhouettes: ©Diego Barneche.

600 **Extended Data Figure 9 | Impacts of long-term warming on C:N ratios.** Mean C:N ratios

601 were calculated from ambient and warmed ponds. Points represent means calculated for the

602 entire duration of the experiment ($n = 8$ per treatment). Boxplots depict the median (mean line),

603 as well as the first and third quartiles (lower and upper hinges). Error whiskers represent up to

604 1.5 times the the inter-quartile range (i.e. distance between the first and third quartiles) beyond

605 the hinges. Shapes represent phytoplankton (top, circles) and zooplankton (squares, bottom).

606 Silhouettes: ©Diego Barneche.

a

b

κ_a (d^{-1})

κ_e (d^{-1})

ϕ (% d)

Efficiency of N transfer ($\bar{\varepsilon}$)

Posterior density (99% C.I.)

Ambient   Warmed

Total Biomass (µg C L^{-1}) vs Treatment (Ambient, Warmed)

Y-axis values: 22000, 3000, 400, 50, 8